Energies and the radiative and Auger transition rates of $1s2p^4$ resonances of B-like ions

Yan Sun, Bing Cong Gou,* and Chao Chen
School of Physics, Beijing Institute of Technology, Beijing 100081, China
(Received 7 January 2013; published 14 March 2013)

Energy levels and the radiative and Auger transition rates of the $1s2p^4\,{}^{2,4}L$ ($L = S$, P, D) resonances in the boron isoelectronic sequence are calculated using the saddle-point variation and saddle-point complex-rotation methods. Large-scale wave functions are used to saturate the functional space. Relativistic and mass polarization corrections are included by the first-order perturbation theory. The Auger branching ratios of the important decay channels for these core-excited states are calculated. The reliable transition wavelengths and Auger electron energies are used to identify available x-ray spectra and Auger electron spectra. Identifications of several unknown experimental lines from $1s2p^4$ resonances are reported. The total radiative rates and total Auger rates of these $1s2p^4$ resonances are also reported and discussed along with the increase of atomic number Z. It is found that the total Auger rates are several orders of magnitude greater than the total radiative rates in these low-Z ions.

DOI: 10.1103/PhysRevA.87.032509 PACS number(s): 31.15.A−, 32.30.Rj, 32.80.Zb

I. INTRODUCTION

In the past few decades, the radiative and Auger transitions of core-excited states of B-like ions have aroused great attention since they are important data related to astrophysics and plasma diagnostics. Several experimental observations [1–8] and theoretical data [8–13] for these core-excited states have been reported. As is well known in Rødbor *et al.* [1–4], the Auger electron spectra of highly excited autoionizing levels of carbon, oxygen, and neon ions were studied by the projectile electrons' collision with rare gases or carbon foil. The x-ray spectra of carbon [5,6], magnesium [7], and silicon [8] ions are observed by foil excitation of fast ion beams and laser-induced plasma experiments. Theoretically, Chen and Crasemann [9,10] calculated radiative and Auger decay properties of the core-excited states in the boron isoelectronic sequence by the multiconfiguration Dirac-Fock (MCDF) method. Using $1/Z$ perturbation theory method and SUPERSTRUCTURE code, Safronova *et al.* [11,12] reported energies and autoionization probabilities of inner-shell excited states of B-like ions with $Z = 6$–54. The self-consistent Hartree-Fock model [13] and R-matrix method [6] were also employed to study the atomic energies and transition properties of B-like ions. However, for the high-lying core-excited $1s2p^4$ configuration states, some discrepancies still exist in these calculated results by different theory models, due to the presence of strong electron correlation effects. In view of the existing discrepancies in these core-excited states, it would be of interest to carry out an accurate calculation so that identifications for some unknown experimental spectrum lines could be made.

In this work, we report energy levels, x-ray wavelengths, radiative rates, Auger electron energies, and Auger rates of the core-excited $1s2p^4\,{}^{2,4}L$ ($L = S$, P, D) states in C^+, O^{3+}, Ne^{5+}, Mg^{7+}, and Si^{9+} ions. Our calculations are carried out by the saddle-point variation and saddle-point complex-rotation methods [14]. The calculated results are compared with available theoretical data and experimental results. The branching ratios of the Auger transition channels for these core-excited $1s2p^4$ configuration states are discussed. Furthermore, calculated x-ray wavelengths and Auger electron energies are used to identify the observed x-ray spectra and high-resolution Auger spectra of B-like ions. Finally, competitive behaviors of total radiative and total Auger rates of these $1s2p^4$ resonances are discussed along with the increase of atomic number Z.

II. COMPUTATIONAL METHOD

In this work, the LS coupling scheme will be used. The Hamiltonian for the B-like system in atomic units is given by

$$H = H_0 + H_1 + H_2 + H_3 + H_4 + H_5, \tag{1}$$

where H_0 is the nonrelativistic Hamiltonian operator:

$$H_0 = \sum_{i=1}^{5}\left[-\frac{1}{2}\nabla_i^2 - \frac{Z}{r_i}\right] + \sum_{\substack{i,j=1\\ i<j}}^{5}\frac{1}{r_{ij}}. \tag{2}$$

$H_1 - H_5$ are the relativistic and mass polarization correction operators:

$$H_1 = -\frac{1}{8c^2}\sum_{i=1}^{5}\boldsymbol{P}_i^4 \quad \text{(kinetic energy correction)}, \tag{3}$$

$$H_2 = \frac{Z\pi}{2c^2}\sum_{i=1}^{5}\delta(\boldsymbol{r}_i) \quad \text{(Darwin term)}, \tag{4}$$

$$H_3 = -\frac{\pi}{c^2}\sum_{\substack{i,j=1\\ i<j}}^{5}\left[1 + \frac{8}{3}\boldsymbol{s}_i\cdot\boldsymbol{s}_j\right]\delta(\boldsymbol{r}_{ij}) \quad \text{(electron−electron contact term)}, \tag{5}$$

$$H_4 = -\frac{1}{2c^2}\sum_{\substack{i,j=1\\ i<j}}^{5}\frac{1}{r_{ij}}\left[\boldsymbol{P}_i\cdot\boldsymbol{P}_j + \frac{\boldsymbol{r}_{ij}(\boldsymbol{r}_{ij}\cdot\boldsymbol{P}_i)\cdot\boldsymbol{P}_j}{r_{i_j}}\right] \quad \text{(retardation potential)}, \tag{6}$$

$$H_5 = -\frac{1}{M}\sum_{\substack{i,j=1\\ i<j}}^{5}\nabla_i\cdot\nabla_j \quad \text{(mass polarization)}. \tag{7}$$

*Corresponding author: goubing@sina.com

 ©2013 American Physical Society

M is the mass of the nucleus and $c = 137.036$. The wave function is the linear combination of basic functions which are the eigenfunctions of L^2, S^2, L_Z, and S_z. The basic wave function of the core-excited B-like system Ψ_b can be written as

$$\Psi_b(1,2,3,4,5) = A\sum_i C_i[1-P_j]\phi_{n(i),l(i)}Y^{LM}_{l(i)}(\Omega)\chi_{SS_z}, \tag{8}$$

where A is the antisymmetrization operator and C_i is the linear coefficient. $\phi_{n(i),l(i)}$ represents the set of possible radial functions, and $Y^{LM}_{l(i)}$ represents the set of possible orbital angular functions. The radial part of the wave function is product of the Slater orbital,

$$\phi_{n(i),l(i)} = \prod_{j=1}^{5} r_j^{n_j}\exp(-\alpha_j r_j). \tag{9}$$

A different set of nonlinear parameters α_j is used for each angular-spin component. The angular part is

$$\begin{aligned} Y^{LM}_{l(i)}(\Omega) = \sum_{m_j} &\langle l_1 l_2 m_1 m_2 | l_{12} m_{12}\rangle \times \langle l_{12} l_3 m_{12} m_3 | l_{123} m_{123}\rangle \\ &\times \langle l_{123} l_4 m_{123} m_4 | l_{1234} m_{1234}\rangle \\ &\times \langle l_{1234} l_5 m_{1234} m_5 | LM\rangle \prod_{j=1}^{5} Y_{l_j m_j}(\Omega_j). \end{aligned} \tag{10}$$

To simplify notation, the angular and spin parts of the wave function can be simply represented by

$$l(i) = \{[(l_1,l_2)l_{12},l_3]l_{123},l_4\}l_{1234},l_5, \tag{11}$$

$$\chi_{SS_z} = \{[(s_1,s_2)s_{12},s_3]s_{123},s_4\}s_{1234},s_5. \tag{12}$$

Here, l_{1234} and l_5 couple into the total orbital angular momentum L; s_{1234} and s_5 couple into the total spin angular momentum S. In this work, for the doublet states, five spin models are possible:

$$\begin{aligned} \chi^1 &= \{[(\tfrac{1}{2},\tfrac{1}{2})0,\tfrac{1}{2}]\tfrac{1}{2},\tfrac{1}{2}\}0,\tfrac{1}{2}, \\ \chi^2 &= \{[(\tfrac{1}{2},\tfrac{1}{2})0,\tfrac{1}{2}]\tfrac{1}{2},\tfrac{1}{2}\}1,\tfrac{1}{2}, \\ \chi^3 &= \{[(\tfrac{1}{2},\tfrac{1}{2})1,\tfrac{1}{2}]\tfrac{1}{2},\tfrac{1}{2}\}0,\tfrac{1}{2}, \\ \chi^4 &= \{[(\tfrac{1}{2},\tfrac{1}{2})1,\tfrac{1}{2}]\tfrac{1}{2},\tfrac{1}{2}\}1,\tfrac{1}{2}, \\ \chi^5 &= \{[(\tfrac{1}{2},\tfrac{1}{2})1,\tfrac{1}{2}]\tfrac{3}{2},\tfrac{1}{2}\}1,\tfrac{1}{2}. \end{aligned} \tag{13}$$

For the quintet states, four spin models are possible:

$$\begin{aligned} \chi^1 &= \{[(\tfrac{1}{2},\tfrac{1}{2})0,\tfrac{1}{2}]\tfrac{1}{2},\tfrac{1}{2}\}1,\tfrac{1}{2}, \\ \chi^2 &= \{[(\tfrac{1}{2},\tfrac{1}{2})1,\tfrac{1}{2}]\tfrac{1}{2},\tfrac{1}{2}\}1,\tfrac{1}{2}, \\ \chi^3 &= \{[(\tfrac{1}{2},\tfrac{1}{2})1,\tfrac{1}{2}]\tfrac{3}{2},\tfrac{1}{2}\}1,\tfrac{1}{2}, \\ \chi^4 &= \{[(\tfrac{1}{2},\tfrac{1}{2})1,\tfrac{1}{2}]\tfrac{3}{2},\tfrac{1}{2}\}2,\tfrac{1}{2}, \end{aligned} \tag{14}$$

In Eq. (8), the projection operator P_j [15] is given by

$$P_j = |\phi_0(r_j)\rangle\langle\phi_0(r_j)|. \tag{15}$$

Here, the vacancy orbital is

$$\phi_0(r) = N\exp(-qr), \tag{16}$$

where q could be described as the effective nuclear charge seen by the vacancy orbital. N is a normalization constant. A set of five nonlinear parameters α_j is chosen for each angular-spin partial wave. The linear coefficients C_i are determined in the energy optimization process. Using the saddle-point variational method [16], the wave function $\Psi_b(1,2,3,4,5)$ is obtained by minimizing E_b with respect to the nonlinear parameters α_j and maximizing E_b with respect to the parameter q. Then, the corresponding resonance nonrelativistic energy becomes

$$E_b = \frac{\langle\Psi_b|H_0|\Psi_b\rangle}{\langle\Psi_b|\Psi_b\rangle}. \tag{17}$$

To saturate the functional space, the restricted variational method [17] is used to further improve the energy E_b. We expand the total wave function as

$$\Phi(1,2,3,4,5) = D_0\Psi_b(1,2,3,4,5) + \Psi_2(1,2,3,4,5), \tag{18}$$

where

$$\Psi_2(1,2,3,4,5) = A\sum_{i=1}^{I} D_i\phi_{n(i),l(i)}(1,2,3,4,5). \tag{19}$$

Ψ_2 is a function to saturate the functional space. D_i's are the linear parameters which can be determined by solving a new secular equation in which the Ψ_b in Eq. (18) is restricted to being a single term; Ψ_2 are basis functions similar to those of Ψ_b. In the restricted variational calculation process, the nonlinear parameters in Ψ_b are fixed. The nonlinear parameters in Ψ_2 are very different from those of Ψ_b. In practice, we will break up Ψ_2 into many parts. They will be calculated individually. Each of the nonlinear parameters in Ψ_2 is optimized in the restricted variational calculation. The improved energy is obtained by

$$\Delta E_{RV} = E_b(\text{new}) - E_b(\text{old}). \tag{20}$$

Then the total nonrelativistic energy is obtained by adding the improvement from restricted variation ΔE_{RV}.

The relativistic and mass polarization corrections are calculated using first-order perturbation theory. Then they are obtained by

$$\Delta E_{\text{rel}} = \langle\Psi_b|H_1 + H_2 + H_3 + H_4|\Psi_b\rangle. \tag{21}$$

$$\Delta E_{\text{mp}} = \langle\Psi_b|H_5|\Psi_b\rangle, \tag{22}$$

The external complex scaling technique [18,19] was implemented by Chung and Davis [20] in connection with the saddle-point technique to describe the open-channel parts of the wave function. Then the resonance states could be described by square integrable eigenfunctions. The energy E_b obtained from the basis wave function is the saddle-point energy. It is a closed-channel approximation of the autoionizing state. To calculate the true resonance energy, we rewrite the total wave function for the resonance including both the closed and open channels,

$$\Psi(1,2,3,4,5) = \Psi_b(1,2,3,4,5) + A\sum_i \phi_i(1,2,3,4)U_i(5), \tag{23}$$

where $\phi_i(1,2,3,4)$ is the target state of the open channels and U_i represents the outgoing electron. The U_i is written as

$$U_i = \sum_n d_{i,n} r^n e^{-\alpha_j r}. \tag{24}$$

In the complex scaling calculation, the radial part r of U_i is complex scaled $r \rightarrow re^{-i\theta}$, with the θ complex scaling angle. The Auger widths are stable values over the range of $\theta = 0.3-0.6$ rad for all the energies tested. In this work, θ is fixed to 0.5 for the entire calculation. In the calculation, the nonlinear parameters in $\Psi_b(1,2,3,4,5)$ are fixed, but the linear parameters are recomputed to allow interaction between the closed-channel and the open-channel wave functions. The complex resonance energy and the width are calculated from the secular equation,

$$E = \frac{\langle \Psi | H | \Psi \rangle}{\langle \Psi | \Psi \rangle}. \tag{25}$$

The energy from $\Psi(1,2,3,4,5)$, $E - \Gamma/2$, gives the position and the width of the resonance. The difference, $\Delta E_S = E - E_b$, represents the shift from the saddle-point energy to the resonance energy due to the interaction between the closed wave function and continua. Then, we obtain the total energy of the core-excited $1s2p^4$ resonance,

$$E_{\text{total}} = E_b + \Delta E_{RV} + \Delta E_S + \Delta E_{\text{mp}} + \Delta E_{\text{rel}}. \tag{26}$$

III. RESULTS AND DISCUSSION

Table I gives resonance energies of these core-excited $1s2p^{4\ 2,4}L$ ($L = S$, P, D) states in B-like C^+, O^{3+}, Ne^{5+}, Mg^{7+}, and Si^{9+} ions. To carry out high-quality calculations of core-excited doublet and quartet systems in B-like ions is challenging work, due to the extremely complex electron correlation effects and the instability in the calculation process. For each set of orbital momenta l_1, l_2, l_3, l_4, l_5, there are several coupling ways to couple this set into the desired total angular momentum. As Eqs. (13) and (14) describe, there are five spin angular coupling modes for the doublet states and four spin models for the quintet states. In order to obtain a reliable result, many relevant angular-spin components must be included in the wave functions. In this work, for the $1s2p^4$ resonances, the important angular series $[l_1l_2l_3l_4l_5]$ is $[011l,l]$, $[011l,l+2]$, $[111l,l+1]$, $[001l,l+1]$, $[000l,l+2]$, $[002l,l]$, $[000l,l]$, [00000], [00002], etc. The number of linear parameters in the basic wave functions ranges from 2520 to 3490 and the number of angular-spin components ranges from 88 to 129. In the process of computation, configuration partial waves with energy contribution less than 1×10^{-5} a.u. are omitted. For these $1s2p^4$ resonances of B-like ions, the absolute energy uncertainty is estimated about 5×10^{-4} a.u. In Table I, E_b is the nonrelativistic energy from the closed-channel wave function. The restricted variational energy improvement ΔE_{RV} ranges from -134 to -384 μ-a.u. The energy shifts ΔE_S are obtained by coupling the important open channels and summing over other channels. In Table I, we note the ΔE_S of ^2D states are larger than those of ^2S

TABLE I. Energies (a.u) of the $1s2p^{4\ 2,4}L$ ($L = S$, P, D) resonances in B-like ions. ΔE_{RV} is the restrictive variation calculation, ΔE_S is the total energy shift, ΔE_{mp} is the mass polarization, ΔE_{rel} is the relativistic correction, and E_{total} is the total energy.

	E_{nonrel}			Corrections		E_{total}	
Resonance	E_b	ΔE_{RV}	ΔE_S	ΔE_{mp}	ΔE_{rel}	Present	Others
				C^+			
$1s2p^4\ ^4P$	−26.213870	−0.000185	0.001186	−0.000152	−0.009573	−26.222594	−26.235503[a]
$1s2p^4\ ^2S$	−25.959582	−0.000216	0.000828	−0.000086	−0.009721	−25.968777	−26.015901[a]
$1s2p^4\ ^2P$	−26.081784	−0.000253	0.001025	0.000008	−0.009812	−26.090816	−26.120082[a]
$1s2p^4\ ^2D$	−26.121626	−0.000285	0.004334	−0.000106	−0.009667	−26.127350	−26.123258[a]
				O^{3+}			
$1s2p^4\ ^4P$	−50.263748	−0.000243	0.001375	−0.000260	−0.032030	−50.294906	
$1s2p^4\ ^2S$	−49.847031	−0.000134	0.000694	−0.000151	−0.032372	−49.878994	
$1s2p^4\ ^2P$	−50.053856	−0.000302	0.001338	0.000018	−0.032813	−50.085615	
$1s2p^4\ ^2D$	−50.107153	−0.000353	0.004974	−0.000174	−0.032374	−50.135080	
				Ne^{5+}			
$1s2p^4\ ^4P$	−82.286491	−0.000232	0.001502	−0.000376	−0.082013	−82.377610	−82.463899[b]
$1s2p^4\ ^2S$	−81.752630	−0.000206	0.001780	−0.000225	−0.082767	−81.834048	−81.887066[b]
$1s2p^4\ ^2P$	−82.021731	−0.000240	0.001533	0.000026	−0.083945	−82.104357	−82.189934[b]
$1s2p^4\ ^2D$	−82.098320	−0.000335	0.006758	−0.000249	−0.082658	−82.174804	−82.241031[b]
				Mg^{7+}			
$1s2p^4\ ^4P$	−122.397861	−0.000215	0.001684	−0.000497	−0.175721	−122.572610	−122.632639[b]
$1s2p^4\ ^2S$	−121.658824	−0.000192	0.001765	−0.000289	−0.177706	−121.835247	−121.893736[b]
$1s2p^4\ ^2P$	−121.992084	−0.000323	0.001654	0.000032	−0.179558	−122.170279	−122.257887[b]
$1s2p^4\ ^2D$	−122.091698	−0.000355	0.008193	−0.000327	−0.177227	−122.261414	−122.334453[b]
				Si^{9+}			
$1s2p^4\ ^4P$	−170.468442	−0.000246	0.001837	−0.000620	−0.334636	−170.802107	−170.772142[b]
$1s2p^4\ ^2S$	−169.560644	−0.000216	0.002029	−0.000372	−0.337982	−169.897185	−169.870441[b]
$1s2p^4\ ^2P$	−169.965989	−0.000348	0.001805	0.000036	−0.340374	−170.304870	−170.296588[b]
$1s2p^4\ ^2D$	−170.088928	−0.000384	0.008970	−0.000408	−0.336893	−170.417643	−170.399414[b]

[a]Reference [6].
[b]Reference [11].

TABLE II. Transition rates (s^{-1}) and wavelengths λ (Å) of the $1s2p^4$ resonances in B-like ions ($Z = 6-14$). Notation a[b] means a × 10^b.

Initial state	Final state	A_l	A_v	A_a	Others	λ Present	λ Others	λ Experiment
				C^+				
$1s2p^4\ ^4P$	$1s^22p^3\ ^4S^o$	1.91[11]	1.93[11]	1.93[11]	2.02[11][a]	43.109	42.819[a],43.146[b]	43.115[b]
$1s2p^4\ ^2S$	$1s^22p^3\ ^2P^o$	6.16[11]	5.81[11]	6.10[11]	4.06[11][a]	42.650	42.440[a],42.750[b]	42.675[b]
$1s2p^4\ ^2P$	$1s^22p^3\ ^2P^o$	3.37[11]	3.30[11]	3.31[11]	3.14[11][a]	43.143	43.181[a],43.172[b]	43.146[b]
	$1s^22p^3\ ^2D^o$	5.17[11]	5.41[11]	5.39[11]	3.10[11][a]	42.728	42.834[b]	42.741[b]
$1s2p^4\ ^2D$	$1s^22p^3\ ^2P^o$	1.04[11]	1.03[11]	1.05[11]	1.02[11][a]	43.293	43.191[b]	43.180[b]
	$1s^22p^3\ ^2D^o$	2.83[11]	3.06[11]	3.08[11]	3.04[11][a]	42.875	42.749[a],42.852[b]	42.853[b]
				O^{3+}				
$1s2p^4\ ^4P$	$1s^22p^3\ ^4S^o$	9.73[11]	9.65[11]	9.75[11]	9.53[11][a]	22.838	22.766[a]	
$1s2p^4\ ^2S$	$1s^22p^3\ ^2P^o$	1.94[12]	1.96[12]	1.94[12]	1.91[12][a]	22.667	22.616[a]	
$1s2p^4\ ^2P$	$1s^22p^3\ ^2P^o$	1.70[12]	1.65[12]	1.67[12]	1.47[12][a]	22.902	22.906[a]	
	$1s^22p^3\ ^2D^o$	2.48[12]	2.61[12]	2.60[12]	2.39[12][a]	22.722		
$1s2p^4\ ^2D$	$1s^22p^3\ ^2P^o$	5.25[11]	5.27[11]	5.34[11]	4.92[11][a]	22.959		
	$1s^22p^3\ ^2D^o$	1.50[12]	1.50[12]	1.51[12]	1.43[12][a]	22.778	22.738[a]	
				Ne^{5+}				
$1s2p^4\ ^4P$	$1s^22p^3\ ^4S^o$	2.75[12]	2.97[12]	3.00[12]	2.89[12][a], 3.45[12][c]	14.069	14.062[a],14.071[c]	
$1s2p^4\ ^2S$	$1s^22p^3\ ^2P^o$	5.94[12]	5.94[12]	6.03[12]	5.78[12][a],7.21[12][c]	14.006	13.987[a],14.016[c]	
$1s2p^4\ ^2P$	$1s^22p^3\ ^2P^o$	4.86[12]	4.94[12]	4.97[12]	4.86[12][a],5.65[12][c]	14.123	14.126[a],14.103[c]	
	$1s^22p^3\ ^2D^o$	7.73[12]	7.82[12]	7.79[11]	7.27[12][a],9.51[12][c]	14.029	14.038[c]	
$1s2p^4\ ^2D$	$1s^22p^3\ ^2P^o$	1.57[12]	1.59[12]	1.62[12]	1.50[12][a],1.76[12][c]	14.154	14.122[c]	
	$1s^22p^3\ ^2D^o$	4.27[12]	4.57[12]	4.61[12]	4.36[12][a],5.29[12][c]	14.060	14.048[a],14.056[c]	
				Mg^{7+}				
$1s2p^4\ ^4P$	$1s^22p^3\ ^4S^o$	6.68[12]	7.12[12]	7.20[12]	6.87[12][a]	9.540	9.528[a]	9.54[d]
$1s2p^4\ ^2S$	$1s^22p^3\ ^2P^o$	1.48[13]	1.46[13]	1.46[13]	1.37[13][a]	9.495	9.487[a]	9.51[d]
$1s2p^4\ ^2P$	$1s^22p^3\ ^2P^o$	1.12[13]	1.16[13]	1.17[13]	1.07[13][a]	9.561	9.563[a]	9.54[d]
	$1s^22p^3\ ^2D^o$	1.85[13]	1.84[13]	1.84[13]	1.66[13][a]	9.507		9.51[d]
$1s2p^4\ ^2D$	$1s^22p^3\ ^2P^o$	3.68[12]	3.78[12]	3.83[12]	3.56[12][a]	9.580		9.61[d]
	$1s^22p^3\ ^2D^o$	1.03[13]	1.08[13]	1.09[13]	1.05[13][a]	9.525	9.520[a]	9.51[d]
				Si^{9+}				
$1s2p^4\ ^4P$	$1s^22p^3\ ^4S^o$	1.38[13]	1.45[13]	1.46[13]	1.41[13][a]	6.881	6.877[a]	6.878[e]
$1s2p^4\ ^2S$	$1s^22p^3\ ^2P^o$	2.92[13]	2.91[13]	2.90[13]	2.80[13][a]	6.844	6.850[a]	6.850[e]
$1s2p^4\ ^2P$	$1s^22p^3\ ^2P^o$	2.30[13]	2.34[13]	2.36[13]	2.17[13][a]	6.886	6.896[a]	6.890[e]
	$1s^22p^3\ ^2D^o$	3.70[13]	3.73[13]	3.71[13]	3.46[13][a]	6.861		6.850[e]
$1s2p^4\ ^2D$	$1s^22p^3\ ^2P^o$	7.45[12]	7.66[12]	7.76[12]	7.27[12][a]	6.898		6.890[e]
	$1s^22p^3\ ^2D^o$	2.24[13]	2.27[13]	2.27[13]	2.15[13][a]	6.873	6.870[a]	6.878[e]

[a]Reference [10].
[b]Reference [6], measurement error bar ± 0.01 Å.
[c]Reference [13].
[d]Reference [7], measurement error bar ± 0.015 Å.
[e]Reference [8].

and $^{2,4}P$ states, and the energy shifts ΔE_S for these $1s2p^4$ resonances increase gradually as Z increases. The relativistic corrections $\Delta E_{\rm rel}$ and the mass polarization $\Delta E_{\rm mp}$ calculated by first-order perturbation theory are also listed in Table I. Then, we obtain the total energies by adding E_b, ΔE_{RV}, ΔE_S, $\Delta E_{\rm mp}$, and $\Delta E_{\rm rel}$. As Table I shows, energy levels of the $1s2p^4$ configuration states of B-like ions in the present work agree with those theoretical results of Jannitti *et al.* [6] and Safronova *et al.* [11].

Calculated transition rates and wavelengths for the $1s2p^4$ resonances of these B-like ions are presented in Table II. In this work, calculated radiative rates from dipole length (A_l), dipole velocity (A_v), and dipole acceleration (A_a) formulae agree well with each other, which indicates the calculated wave functions are accurate. For example, A_l, A_v, and A_a of the transition $1s2p^4\ ^4P \rightarrow 1s^22p^3\ ^4S^o$ in C^+ ion are 1.91×10^{11}, 1.93×10^{11}, and 1.93×10^{11}, respectively. Also, our calculated radiative rates are in good agreement with the theoretical results of Chen and Crasemann [10] and Karim and Logan [13]. In this work, for these B-like ions, the quantum-electrodynamic effect and high-order relativistic corrections for transition wavelengths are about 0.004 Å by the formula in Refs. [21,22], which are smaller than the experimental uncertainties. So they are not considered in the wavelength calculations. To compare, our calculated wavelengths together with other theoretical predictions [6,10,13] and experimental results [6–8] are also given in this Table. The calculated results are in good agreement with experiments. For the transition $1s2p^4\ ^4P \rightarrow 1s^22p^3\ ^4S^o$ of C^+ ion, our calculated wavelength 43.109 Å agrees well with the observed experimental result

TABLE III. Partial Auger rates W_A (s^{-1}), branching ratios (BR), Auger electron energies (eV), and the identified experimental lines of the $1s2p^4$ resonances in B-like ions. Notation a[b] means a $\times 10^b$. The number in parentheses indicates the experimental line number.

					Auger electron energy (eV)			
		W_A				Others		
Resonance	Channel	Present	Ref. [10]	BR (%)	Present	Ref. [10]	Ref. [24]	Experiment
				C^+				
$1s2p^4\,^2S$	$1s^22s^2\,^1S$	4.86[12]	2.60[11]	3.1	287.87	291.89		
	$1s^22p^2\,^1S$	3.95[13]	1.30[13]	25.5	265.22	267.45		$265.3 \pm 0.5(29)$[b]
	$1s^22p^2\,^1D$	1.09[14]	6.73[13]	70.2	269.76	272.49		$270.0 \pm 0.7(34)$[b]
	$1s^22s2p\,^1P^o$	1.55[12]	2.46[12]	1.0	275.16	277.75		
	$1s^22s2p\,^3P^o$	2.74[11]	1.44[12]	0.2	281.36			
$1s2p^4\,^2P$	$1s^22p^2\,^1D$	2.31[10]	2.66[9]	0	266.44	267.47		$266.6 \pm 0.7(30)$[b]
	$1s^22p^2\,^3P$	1.30[14]	7.59[13]	99.5	267.50	274.59		$267.5 \pm 0.7(31)$[b]
	$1s^22s2p\,^1P^o$	5.34[11]	5.04[11]	0.4	271.84	272.73		$272.1 \pm 0.7(35)$[b]
	$1s^22s2p\,^3P^o$	1.00[11]	7.73[9]	0.1	278.04	285.27		$278.7 \pm 0.7(39)$[b]
$1s2p^4\,^2D$	$1s^22s^2\,^1S$	2.67[12]	5.46[9]	1.3	283.55	286.87	285.13	
	$1s^22p^2\,^1S$	2.37[13]	1.65[13]	11.4	260.90	262.42	264.56	$261.82 \pm 0.2(27)$[b]
	$1s^22p^2\,^1D$	1.80[14]	1.06[14]	86.7	265.44	267.46	266.61	$265.3 \pm 0.5(29)$[b]
	$1s^22p^2\,^3P$	1.18[10]	1.15[9]	0	266.50		269.75	$266.6 \pm 0.7(30)$[b]
	$1s^22s2p\,^1P^o$	9.12[11]	7.78[11]	0.4	270.84	272.72	272.96	
	$1s^22s2p^3P^o$	2.46[11]	4.75[11]	0.1	277.05		280.43	
$1s2p^4\,^4P$	$1s^22s2p\,^3P^o$	3.07[11]	1.65[12]	0.3	274.45		276.08	$274.1 \pm 0.7(37)$[b]
	$1s^22p^2\,^3P$	1.21[14]	7.70[13]	99.7	263.91		265.40	$263.71 \pm 0.7(28)$[b]
								$263.8 \pm 0.6(28)$[c]
				O^{3+}				
$1s2p^4\,^2S$	$1s^22s^2\,^1S$	5.46[12]	2.92[11]	2.1	505.62	509.54		
	$1s^22p^2\,^1S$	4.25[13]	2.11[13]	16.6	469.88	471.97		471(10)[d]
	$1s^22p^2\,^1D$	2.02[14]	1.08[14]	79.1	476.84	479.46		$477 \pm 2(9')$[d]
	$1s^22s2p\,^1P^o$	4.35[12]	3.43[12]	1.7	485.88	488.26		$486 \pm 2(11')$[d]
	$1s^22s2p^3P^o$	9.75[11]	1.48[12]	0.4	495.40	499.21		
$1s2p^4\,^2P$	$1s^22p^2\,^1D$	4.56[9]	2.53[11]	0	471.22	472.51		471(10)[d]
	$1s^22p^2\,^3P$	2.21[14]	1.20[14]	99.7	473.48			471(10)[d]
	$1s^22s2p\,^1P^o$	4.47[11]	4.95[11]	0.2	480.26	481.32		481(11)[d],$481 \pm 2(10')$[d]
	$1s^22s2p\,^3P^o$	2.18[11]	5.62[10]	0.1	489.78			$490 \pm 2(12')$[d]
$1s2p^4\,^2D$	$1s^22s^2\,^1S$	4.43[12]	7.22[9]	1.3	498.65	502.07		
	$1s^22p^2\,^1S$	4.71[13]	2.57[13]	13.4	462.91	464.50		$463 \pm 2(8)$[d]
	$1s^22p^2\,^1D$	2.98[14]	1.68[14]	84.8	469.87	471.98		471(10)[d]
	$1s^22p^2\,^3P$	7.60[9]	1.32[11]	0	472.13			471(10)[d]
	$1s^22s2p\,^1P^o$	1.45[12]	1.05[12]	0.4	478.91	480.79		$477 \pm 2(9')$[d]
	$1s^22s2p\,^3P^o$	3.00[11]	4.73[11]	0.1	488.43			$486 \pm 2(11')$[d]
$1s2p^4\,^4P$	$1s^22s2p\,^3P^o$	1.98[12]	2.04[12]	1.0	484.08			484(12)[d]
	$1s^22p^2\,^3P$	2.05[14]	1.29[14]	99.0	467.78			$466 \pm 2(9)$[d]
				Ne^{5+}				
$1s2p^4\,^2S$	$1s^22s^2\,^1S$	6.68[12]	3.06[11]	2.1	777.86	781.80		
	$1s^22p^2\,^1S$	4.98[13]	2.68[13]	15.7	729.08	731.16		
	$1s^22p^2\,^1D$	2.54[14]	1.37[14]	80.0	738.39	741.05		
	$1s^22s2p\,^1P^o$	5.77[12]	4.05[12]	1.8	751.12	753.50		
	$1s^22s2p\,^3P^o$	1.23[12]	1.50[12]	0.4	763.92	767.75		
$1s2p^4\,^2P$	$1s^22p^2\,^1D$	2.89[9]	1.01[12]	0	731.03	732.31		
	$1s^22p^2\,^3P$	2.74[14]	1.51[14]	99.7	734.48	736.80		
	$1s^22s2p\,^1P^o$	5.44[11]	4.91[11]	0.2	743.76	744.76		
	$1s^22s2p\,^3P^o$	3.04[11]	1.04[11]	0.1	756.57			
$1s2p^4\,^2D$	$1s^22s^2\,^1S$	6.41[12]	7.91[9]	1.4	768.58	771.94		
	$1s^22p^2\,^1S$	5.47[13]	3.21[13]	11.9	719.81	721.29		
	$1s^22p^2\,^1D$	3.95[14]	2.12[14]	86.1	729.11	731.18		729.61[e]
	$1s^22p^2\,^3P$	7.74[9]	5.55[11]	0	732.56			731.77[e]
	$1s^22s2p\,^1P^o$	2.01[12]	1.23[12]	0.4	741.84	743.63		741.65[e]
	$1s^22s2p\,^3P^o$	4.25[11]	4.69[11]	0.1	754.65			
$1s2p^4\,^4P$	$1s^22s2p\,^3P^o$	2.85[12]	2.28[12]	1.0	749.41			
	$1s^22p^2\,^3P$	2.86[14]	1.54[14]	99.0	727.32	728.40		727.91[e]

TABLE III. (*Continued.*)

					Auger electron energy (eV)			
		W_A				Others		
Resonance	Channel	Present	Ref. [10]	BR (%)	Present	Ref. [10]	Ref. [24]	Experiment
				Mg^{7+}				
$1s2p^4\,^2S$	$1s^22s^2\,^1S$	6.98[12]	3.11[11]	1.9	1105.27	1109.11		
	$1s^22p^2\,^1S$	5.18[13]	3.10[13]	14.2	1043.28	1045.23		
	$1s^22p^2\,^1D$	2.98[14]	1.59[14]	81.7	1054.94	1057.50		
	$1s^22s2p\,^1P^o$	6.68[12]	4.41[12]	1.8	1071.48	1073.72		
	$1s^22s2p\,^3P^o$	1.47[12]	1.49[12]	0.4	1087.53	1091.25		
$1s2p^4\,^2P$	$1s^22p^2\,^1D$	5.77[9]	3.29[12]	0	1045.83	1047.01		
	$1s^22p^2\,^3P$	3.31[14]	1.73[14]	99.7	1050.44			
	$1s^22s2p\,^1P^o$	5.77[11]	4.86[11]	0.2	1062.36	1063.23		
	$1s^22s2p\,^3P^o$	3.68[11]	1.40[11]	0.1	1078.41			
$1s2p^4\,^2D$	$1s^22s^2\,^1S$	7.90[12]	8.08[9]	1.5	1093.67	1096.85		
	$1s^22p^2\,^1S$	6.28[13]	3.66[13]	11.9	1031.69	1032.98		
	$1s^22p^2\,^1D$	4.53[14]	2.43[14]	86.0	1043.35	1045.25		
	$1s^22p^2\,^3P$	5.77[9]	1.87[12]	0	1047.96			
	$1s^22s2p\,^1P^o$	2.32[12]	1.32[12]	0.4	1059.88	1061.47		
	$1s^22s2p\,^3P^o$	4.98[11]	4.61[11]	0.1	1075.93			
$1s2p^4\,^4P$	$1s^22s2p\,^3P^o$	3.25[12]	2.40[12]	0.9	1067.46			
	$1s^22p^2\,^3P$	3.40[14]	1.78[14]	99.1	1039.49			
				Si^{9+}				
$1s2p^4\,^2S$	$1s^22s^2\,^1S$	7.60[12]	3.11[11]	1.9	1488.35	1491.86		
	$1s^22p^2\,^1S$	5.46[13]	3.42[13]	13.5	1412.84	1414.45		
	$1s^22p^2\,^1D$	3.34[14]	1.75[14]	82.4	1426.86	1429.08		
	$1s^22s2p\,^1P^o$	7.59[12]	4.64[12]	1.9	1447.38	1449.27		
	$1s^22s2p\,^3P^o$	1.58[12]	1.51[12]	0.4	1466.62			
$1s2p^4\,^2P$	$1s^22p^2\,^1D$	1.58[9]	8.95[12]	0	1415.77	1416.87		
	$1s^22p^2\,^3P$	3.77[14]	1.85[14]	99.7	1421.53			
	$1s^22s2p\,^1P^o$	5.89[11]	4.99[11]	0.2	1436.29	1437.05		
	$1s^22s2p\,^3P^o$	4.86[11]	1.64[11]	0.1	1455.53			
$1s2p^4\,^2D$	$1s^22s^2\,^1S$	8.20[12]	7.84[9]	1.4	1474.19	1477.20		
	$1s^22p^2\,^1S$	6.68[13]	3.94[13]	11.1	1398.68	1399.78		
	$1s^22p^2\,^1D$	5.23[14]	2.63[14]	87.0	1412.70	1414.42		
	$1s^22p^2\,^3P$	3.95[9]	5.27[12]	0.0	1418.46			
	$1s^22s2p\,^1P^o$	2.44[12]	1.38[12]	0.4	1433.22	1434.60		
	$1s^22s2p\,^3P^o$	5.70[11]	4.61[11]	0.1	1452.46			
$1s2p^4\,^4P$	$1s^22s2p\,^3P^o$	3.72[12]	2.49[12]	1.0	1442.00			
	$1s^22p^2\,^3P$	3.80[14]	1.95[14]	99.0	1408.00			

[a]Reference [10].
[b]Reference [24].
[c]Reference [1].
[d]Reference [2]. Lines 8 −12 are 2-MeV spectrum lines. Lines 9′ −12′ are 5-MeV spectrum lines.
[e]Reference [4].

43.115 Å [6]. The predicted wavelength 42.650 Å for the transition $1s2p^4\,^2S \rightarrow 1s^22p^3\,^2P^o$ is in good agreement with the experiment result 42.675 Å [6]. Also, for the transitions $1s2p^4\,^2P \rightarrow 1s^22p^3\,^2P^o$ and $1s2p^4\,^2P \rightarrow 1s^22p^3\,^2D^o$ of B-like carbon ion, our prediction of 43.143 and 42.728 Å agrees with the experimental lines [6] at 43.146 and 42.741 Å, respectively. Armour *et al.* [7] and Träbert and Fawcett [8] reported the x-ray spectra lines of magnesium and silicon ions and pointed out some lines may arise from the radiative transitions of the core-excited states in Mg^{7+} and Si^{9+} ions. Here, we give detailed identifications for these experimental optical spectra lines in the last column of Table II. For the x-ray spectrum of Mg ions, the lines at 9.51, 9.54, and 9.61 Å could be from radiative transitions of the core-excited $1s2p^4$ states. Three lines at 6.850, 6.878, and 6.890 Å in Si^{9+} ion are also identified.

In Table III, we present partial Auger rates, Auger branching ratios (BR), and corresponding Auger electron energies of the $1s2p^4$ resonances in B-like ions. The "hollow" core-excited $1s2p^4$ resonances lie above multiple ionization threshold and may decay through many different Auger channels. In this work, we compute Auger rates for the selected important channels by the saddle-point complex-rotation method. As Table III shows, the Auger rates in the present work are in

agreement with the theoretical results of Chen and Crasemann [10]. The Auger decay process involves the energy exchange between two excited electrons through Coulomb interaction. For the $1s2p^4$ resonances, the major interaction comes from two $2p$ electrons. One $2p$ electron falls into the $1s$ inner-shell vacancy and transfers residual energy to the other $2p$ electron, whereas the other $2p$ receives the energy and escapes from the system, leaving a $1s^22p^2$ configuration state. Hence, the $1s^22p^2\ ^1S$, $1s^22p^2\ ^1D$, $1s^22p^2\ ^3P$ states should be the major Auger channels and these channels should have large branching ratios. For the wave functions of $1s2p^4$ resonances, the most important angular-spin component is *spppp*. The mixed *ssspp* angular-spin component also occupies a large part. For example, in the normalization of angular-spin components of the $1s2p^4\ ^2S$ wave function of C^+ ion, the contribution of the *spppp* component is 80.5% and that of *ssspp* is 12.6%. For the $1s2p^4\ ^4P$ states of C^+ ion, the contribution of the *spppp* component is 86.1% and that of *ssspp* is 7.5%. Therefore, we also calculated the Auger rates for $1s^22s^2\ ^1S$, $1s^22s2p\ ^1P^o$, $1s^22s2p^3P^o$ target states as they may decay from the interacted $1s2s^22p^2$ resonances in the wave functions of $1s2p^4$ resonances. As can be seen from Table III, the branching ratios for the transition channels of these $1s2p^4$ resonances are consistent with our discussions above.

In this work, we have adopted a large-scale basis set and further considered the energy shifts due to the interaction between the closed wave function and continua. The accurate Auger energies and Auger branching ratios enable us to make identifications in the high-resolution Auger spectra. In this work, some experimental lines from the observed Auger electron spectra [1,2,4] are identified and the identified experimental lines are listed in the last column of Table III. As Table III shows, the uncertainties of calculated Auger energies between the present results and experimental measurements are smaller than 0.6%. In an earlier work [23], we identified some lines in the range of 238–277 eV in 300-keV $C^+ \rightarrow CH_4$ collision Auger spectrum as coming from Auger transitions of the core-excited $1s2s^22p^2$ and $1s2s2p^3$ resonances in C^+ ion. In this work, the experimental lines in the range of 261–280 eV are indentified from Auger transitions of the $1s2p^4$ resonances. We have identified line 31 from 300-keV $C^+ \rightarrow CH_4$ collision spectrum [1]. Line 31 was reported at 267.5 ± 0.7 eV. Our calculated Auger energy 267.50 eV for the Auger transition $1s2p^4\ ^2P \rightarrow 1s^22p^2\ ^3P$ agrees well with this observed line position. The Auger transition $1s2p^4\ ^2D \rightarrow 1s^22p^2\ ^1D$ was assigned for line 30 reported at 266.6 ± 0.7 eV in Ref. [24]. However, our calculated result shows that the predicted Auger electron energy 265.44 eV for this transition is close to the line 29 position 265.3 ± 0.5 eV. So we reassign the Auger transition $1s2p^4\ ^2D \rightarrow 1s^22p^2\ ^1D$ for line 29. In Ref. [2], the 2- and 5-MeV projectile Auger spectra were expected to be dominated by four-, five-, and six-electron oxygen ions. In this work, we identify lines 8–12 in 2-MeV spectra and 9′–12′ in 5-MeV spectra as coming from the Auger decay of five-electron core-excited $1s2p^4$ states in O^{3+} ion. Lines 8 and 9 reported at 463 ± 2 eV and 466 ± 2 eV agree well with our prediction of 462.91 eV for transition $1s2p^4\ ^2D \rightarrow 1s^22p^2\ ^1S$ and 467.78 eV for transition $1s2p^4\ ^4P \rightarrow 1s^22p^2\ ^3P$, respectively. The experimental line 10 was observed at 471 eV. Our results suggest that it could be an overlap of three Auger channels, namely,

$$1s2p^4\ ^2D \rightarrow 1s^22p^2\ ^1D \text{ (469.87 eV)},$$
$$1s2p^4\ ^2P \rightarrow 1s^22p^2\ ^3P \text{ (473.48 eV)},$$
$$1s2p^4\ ^2S \rightarrow 1s^22p^2\ ^1S \text{ (469.88 eV)}.$$

Table III also shows that line 11 reported at 481 eV corresponds to the transition $1s2p^4\ ^2P \rightarrow 1s^22s2p\ ^1P^o$ predicted at 480.26

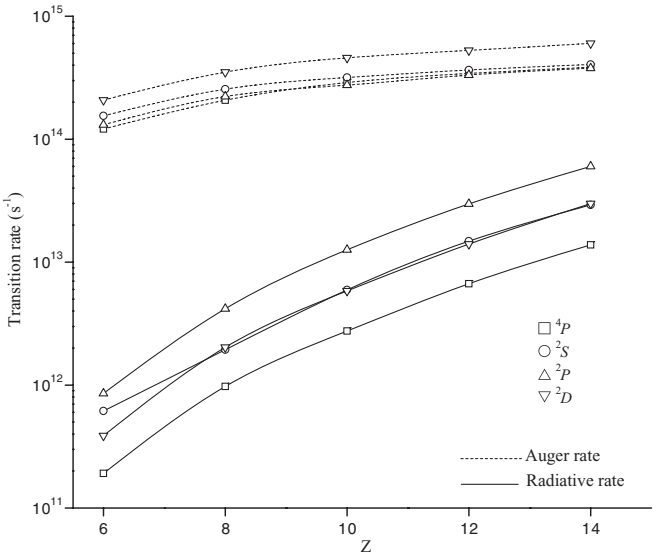

FIG. 1. Total radiative rates and total Auger rates for the core-excited $1s2p^4$ resonances of the boron isoelectronic sequence.

TABLE IV. Total radiative and total Auger rates of the $1s2p^4$ resonances in the boron isoelectronic sequence. R is total radiative rate; A is total Auger rate. Notation a[b] means a $\times 10^b$.

	^4P		^2S		^2P		^2D	
Ions	R	A	R	A	R	A	R	A
C^+	1.91[11]	1.21[14]	6.16[11]	1.55[14]	8.54[11]	1.31[14]	3.87[11]	2.08[14]
O^{3+}	9.73[11]	2.07[14]	1.94[12]	2.55[14]	4.18[12]	2.22[14]	2.03[12]	3.51[14]
Ne^{5+}	2.75[12]	2.89[14]	5.94[12]	3.17[14]	1.26[13]	2.75[14]	5.84[12]	4.59[14]
		1.71[14][a]		2.11[14][a]		1.72[14][a]		2.66[14][a]
Mg^{7+}	6.68[12]	3.43[14]	1.48[13]	3.65[14]	2.97[13]	3.32[14]	1.40[13]	5.27[14]
Si^{9+}	1.38[13]	3.84[14]	2.92[13]	4.05[14]	6.00[13]	3.78[14]	2.99[13]	6.01[14]

[a]Reference [13].

eV and line 12 reported at 484 eV corresponds to the transition $1s2p^4\ ^4P \rightarrow 1s^2 2s2p\ ^3P^o$ at 484.08 eV. The detailed identifications for lines 9′–12′ of 5-MeV oxygen spectra are also listed in Table III. For the Auger transitions of Ne^{5+} ion, the transition $1s2p^4\ ^4P \rightarrow 1s^2 2p^2\ ^3P$ is assigned for the experimental line at 727.91 eV, which supports the identification of Kádár *et al.* [4]. The transition $1s2p^4\ ^2D \rightarrow 1s^2 2p^2\ ^1D$ was assigned for the observed line at 731.77 eV in Ref. [4]. However, our calculated Auger energy for this transition 729.11 eV is close with the unidentified line observed at 729.61 eV. Therefore, we reassign the transition $1s2p^4\ ^2D \rightarrow 1s^2 2p^2\ ^1D$ to the experimental line at 729.61 eV. The line at 731.77 eV [4] is identified as coming from the Auger transition $1s2p^4\ ^2D \rightarrow 1s^2 2p^2\ ^3P$ at 732.56 eV.

Total radiative rates and total Auger rates of the $1s2p^4$ resonances in the boron isoelectronic sequence are listed in Table IV. Our calculated total radiative rates and total Auger rates agree well with those results of Karim and Logan [13] of B-like Ne^{5+} ion. Figure 1 shows the changes of total radiative rates and total Auger rates along with the increase of atomic number Z. As can be seen from Fig. 1, the total Auger rates are several orders of magnitude greater than the total radiative rates in low-Z ions. The total radiative rates increase faster than the total Auger rates. Therefore, the total radiative rates will be greater than the total Auger rates in high-Z ions. Our theoretical results could be valuable for future experiments.

IV. CONCLUSIONS

In this work, the core-excited $1s2p^4$ resonances of the boron isoelectronic sequence (Z = 6–14) are studied. The energy shifts, relativistic corrections, and mass polarization effects are taken into account to obtain reliable energy results. Energy levels, radiative rates, and Auger rates for these states are reported and compared with available theoretical and experimental results. Good agreement is obtained between our calculated x-ray wavelengths and those of experimental data. The Auger spectra lines from the collision experiments [1,2,4] are identified by calculated Auger electron energies and Auger branching ratios. Especially, several unidentified lines in the Auger spectra lines of carbon and neon ions are identified. Competitive behaviors of total radiative and total Auger rates for these core-excited $1s2p^4$ configuration states are discussed along with the increase of Z. It is found that the total Auger rates are significantly greater than the total radiative rates in low-Z ions, and the total radiative rates will be greater than the total Auger rates in high-Z ions.

ACKNOWLEDGMENTS

The authors are grateful to Dr. Kwong T. Chung for the computer code. This work was supported by the National Natural Science Foundation of China under Grant No. 11074022.

[1] M. Rødbor, R. Bruch, and B. Bisgaard, J. Phys. B **12**, 2413 (1979).
[2] R. Bruch, D. Schneider, W. H. E. Schwarz, M. Meinhart, B. M. Johnson, and K. Taulbjerg, Phys. Rev. A **19**, 587 (1979).
[3] A. Itoh, D. Schneider, T. Schneider, T. J. M. Zouros, G. Nolte, G. Schiwietz, W. Zeitz, and N. Stolterfoht, Phys. Rev. A **31**, 684 (1985).
[4] I. Kádár, S. Ricz, J. Végh, B. Sulik, D. Varga, and D. Berényi, Phys. Rev. A **41**, 3518 (1990).
[5] J. R. Huddle and J. R. Mowat, Phys. Rev. A **25**, 1192 (1982).
[6] E. Jannitti, M. Gaye, M. Mazzoni, P. Nicolosi, and P. Villoresi, Phys. Rev. A **47**, 4033 (1993).
[7] I. A. Armour, B. C. Fawcett, J. D. Silver, and E. Träbert, J. Phys. B **13**, 2701 (1980).
[8] E. Träbert and B. C. Fawceet, J. Phys. B **12**, L441 (1979).
[9] M. H. Chen and B. Crasemann, Phys. Rev. A **35**, 4579 (1987).
[10] M. H. Chen and B. Crasemann, At. Data Nucl. Data Tables **38**, 381 (1988).
[11] U. I. Safronova and A. S. Shlyaptseva, Phys. Scr. **54**, 254 (1996).
[12] U. I. Safronova, A. S. Shlyaptseva, M. Cornille, and J. Dubau, Phys. Scr. **57**, 395 (1998).
[13] K. R. Karim and L. Logan, Phys. Scr. **58**, 574 (1998).
[14] K. T. Chung, Phys. Rev. A **20**, 1743 (1979).
[15] K. T. Chung and B. F. Davis, Phys. Rev. A **22**, 835 (1980).
[16] K. T. Chung and B. F. Davis, *Autoionization, Recent Developments and Applications,* edited by A. Temkin (Plenum Press, New York, 1985), p. 73.
[17] K. T. Chung and X. W. Zhu, Phys. Rev. A **48**, 1944 (1993).
[18] J. Aguilar and J. M. Combes, Commun. Math. Phys. **22**, 269 (1971).
[19] C. W. McCurdy and T. N. Rescigno, Phys. Rev. A **62**, 032712 (2000).
[20] K. T. Chung and B. F. Davis, Phys. Rev. A **26**, 3278 (1982).
[21] K. T. Chung, X. W. Zhu, and Z. W. Wang, Phys. Rev. A **47**, 1740 (1993).
[22] Y. Sun, F. Chen, L. Zhuo, and B. C. Gou, Int. J. Quantum Chem. **112**, 1114 (2012)
[23] Y. Sun, F. Chen, and B. C. Gou, J. Chem. Phys. **135**, 124309 (2011).
[24] R. Bruch, K. T. Chung, W. L. Luken, and J. C. Culberson, Phys. Rev. A **31**, 310 (1985).